Cholinergic Signaling Modulates Intestinal Pathophysiology in a *Drosophila* Model of Cystic Fibrosis

Elizabeth A. Lane[1,*], Afroditi Petsakou[1], Ying Liu[1], Weihang Chen[1], Mujeeb Qadiri[1], Yanhui Hu[1], Norbert Perrimon[1,2,*]

Affiliations:
[1] Department of Genetics, Blavatnik Institute, Harvard Medical School, Boston, MA, 7 02115, USA
[2] HHMI, Harvard Medical School, Boston, MA, 02115, USA

*Corresponding authors

Abstract

Cystic fibrosis (CF) is a monogenic genetic disease caused by mutations in the Cystic Fibrosis Transmembrane conductance Regulator (CFTR) chloride/bicarbonate channel, which is expressed in certain epithelial cells. Current therapies focus on restoring CFTR function, but many gut-related pathologies persist, highlighting the need for complementary treatments to improve the quality of life of people with CF. In this study, we use *Drosophila melanogaster* as a model to investigate the gut-specific effects of *Cftr* loss. We demonstrate that enterocyte specific knockdown of *Cftr* in flies recapitulates several CF pathologies, including reduced intestinal motility, nutrient malabsorption, and decreased energy stores. Using single-nuclei RNA sequencing (snRNA-seq), we identify significant transcriptional changes in the CF model gut, including the upregulation of *acetylcholine esterase* (*Ace*, human *AChE*), which leads to reduced cholinergic signaling. Cholinergic signaling has been shown to affect CFTR function but this is the first time CFTR loss of function has been shown to alter cholinergic signaling. Functional assays confirm that cholinergic sensitivity is diminished in CF guts. Furthermore, restoring cholinergic signaling via *Ace* knockdown rescues multiple CF-associated phenotypes. Additionally, we identify the transcription factor Fork head (Fkh), the *Drosophila* homolog of human FOXA1/FOXA2, which is known to be a positive regulator of *Cftr* transcription in the

intestine, as a positive regulator of *Ace* expression in CF guts. This study establishes the *Drosophila* gut as a powerful model to investigate CF pathogenesis, genetic modifiers, and identifies *Ace* and *fkh* as genetic modifiers. This work also suggests that enhancing cholinergic signaling may represent a viable therapeutic strategy for gastrointestinal manifestations of CF.

Author Summary

Cystic fibrosis (CF) is a genetic disease that causes complications in multiple organ systems, including the lungs and gastrointestinal tract. While recent therapies have greatly improved life span and respiratory outcomes in people with CF (pwCF), they continue to report significant gastrointestinal symptoms that impact their quality of life. Therefore, there is a need to better understand the progression of CF in the gut and identify gut specific therapeutic targets to improve patient quality of life. In this study we use *Drosophila* to model gut specific complications of CF. We show our model recapitulates many CF clinical presentations in the gut demonstrating our model may be clinically relevant. Furthermore, we identify *acetylcholine esterase* (*Ace*) as a gene that is increased in our CF model guts that is important for the development of CF pathologies. We additionally, perform a screen to identify a transcriptional regulator of *Ace*, whose genetic manipulation also regulates CF phenotypes. Our findings not only identify a potential target to alleviate GI symptoms in patients with CF, but also validate the *Drosophila* gut as a robust model for studying CF pathogenesis, genetic modifiers, and screening therapeutics.

Introduction

Cystic fibrosis (CF) is a genetic disease that affects approximately 1 in 2,500 newborns in the United States(1). CF is caused by mutations in the Cystic Fibrosis Transmembrane conductance Regulator (CFTR) chloride channel, which is expressed in certain epithelial tissues, including the respiratory tract, pancreas, and the gut(2-4). The CF phenotype is most closely associated with the accumulation of mucus in the pulmonary and gastrointestinal tracts, which can lead to inflammation, bacterial infection, and malnutrition(1, 5-8). Much of CF research has focused on the lung, as the primary cause of death in people with CF (pwCF) have been related to lung complications, however, CF causes pathologies in other CFTR-expressing tissues, including the gut, that result in various clinical phenotypes(7, 9-13). For example, many pwCF are born with intestinal blockage (Meconium Ileus) and later in life have decreased intestinal motility, dysbiosis, inflammation, and poor nutrient absorption in the gut(7, 9-13). Additionally, as life expectancy has increased following better treatments, complications in the gastrointestinal tract have become an increasing cause of morbidity(10-15). These complications include small bowel bacterial overgrowth, bowel obstructions, and increased risk of intestinal cancers(11-13). Recent studies have suggested that CF modulator drugs may not fully correct the inflammation and dysbiosis seen in the gut of pwCF and that pwCF on modulator drugs still report GI symptoms(14, 16-19). Therefore, additional therapies targeting the gut, not directly related to modulating CF activity may be useful for quality of life of pwCF. Recently, there have been studies highlighting how the CF gut can crosstalk with many other organ systems, further highlighting the importance of investigating how loss of CFTR function effects gut biology(20-22).

The *Drosophila* midgut, analogous to the human intestine, is comprised primarily of 4 main cell types: the absorptive enterocytes (ECs), the neuropeptide producing enteroendocrine

(EE) cells, intestinal stem cells (ISCs), and the intermediate progenitor enteroblasts (EBs) (23). The *Drosophila* midgut has been used to study a number of questions in stem cell biology, cell signaling, and physiology, and many of the mechanisms active in the intestines of flies have already been shown to apply more broadly to other organisms and may therefore be relevant for human pathologies(23-25). The fly ortholog of human CFTR has recently been identified and used to establish an intestinal CF model(26). This model revealed that *Cftr* knockdown in the *Drosophila* intestine disrupts osmotic homeostasis and displays CF-like phenotypes in the intestinal epithelium(26). While this work introduced *Drosophila* as a CF model, the phenotypes examined were largely cellular phenotypes, such as increased chloride and sodium levels in the ECs, and not clinical manifestations of CF.

Here, we further characterize the CF model gut, demonstrating that several clinical pathologies, including reduced intestinal motility and nutrient malabsorption are preserved. Furthermore, the *Drosophila* CF model displays characteristics consistent with a failure to thrive phenotype. Additionally, we perform single nuclei RNA-seq (snRNA-seq) to further characterize the CF gut model and learn new biology relevant to CF. Interestingly, we found increased *acetylcholine esterase* (*Ace*) expression in CF model guts, which results in reduced cholinergic signaling potential. Recent work in *Drosophila* has demonstrated that cholinergic signaling is important for maintenance of the intestinal epithelial barrier and is required for the intestinal epithelium to return to homeostasis after injury(27, 28). Additionally cholinergic signaling has been implicated in other diseases of intestinal inflammation such as Inflammatory Bowel Disease (IBD) but has not yet been investigated in the context of the CF intestine(29, 30). Previous studies have demonstrated that cholinergic signaling can increase CFTR function(31-34) but this is the first work that demonstrates CFTR function can have a reciprocal effect on cholinergic

signaling. We further show that the decrease in cholinergic signaling observed in the CF model guts may be clinically relevant as restoring sensitivity to cholinergic signaling rescues many CF pathologies in *Drosophila*. Finally, we identify Fork head (Fkh), a FOXA1/A2 homolog as a transcriptional regulator of *Ace* expression in the CF model gut. FOXA1/A2 is a pioneering transcription factor that positively regulates the expression of *Cftr* and other transmembrane proteins and ion channels important for regulating ion homeostasis in the intestinal epithelium(35, 36). Altogether, our findings help establish *Drosophila* as a model organism to study GI manifestations of CF. We identify Ace (human: AChE) and Fkh (human: FOXA1/A2) as genetic modifiers of CF and our findings suggests that the cholinergic signaling pathway may be a viable therapeutic target in CF gastrointestinal disease.

Results

Knockdown of *Cftr* in the *Drosophila* midgut recapitulates clinical pathologies of Cystic Fibrosis

People with CF (pwCF) display a range of multiple organ specific as well as systemic pathologies, including gastrointestinal complications(10-13, 37-39). Therefore, we examined whether *Drosophila* CF model guts, with enterocyte-specific knockdown of *Cftr* (*Myo1A-Gal4* > *UAS-Cftr*^{RNAi}) recapitulated typical clinical pathologies. pwCF are at increased risk for gastrointestinal cancers and microbial dysbiosis(11, 13, 39, 40). These clinical observations are consistent with previous findings in the *Drosophila* CF model, showing gut hyperplasia and increased bacterial load(26). Additional common CF gut pathologies such as meconium ileus, distal intestinal obstruction syndrome, and constipation are linked to impaired intestinal motility(9, 38, 41). To test whether the CF model exhibits reduced gut motility, we performed an

excretion assay. *Cftr* knockdown flies showed significantly reduced excretion compared to wild-type (WT) controls, indicating impaired intestinal transit (Fig 1A, S1A). Malabsorption of nutrients in the intestine is another hallmark of CF(42). In line with this, CF model flies exhibited increased glucose, triacyl glycerides (TAGs), and protein levels in their excreta compared to WT flies, suggesting reduced nutrient absorption in the intestine (Fig 1B-D, S1B). Of note increased tissue breakdown and stress responses can result in the fly kidney (Malpighian tubules) depositing lipids into the excreta which may contribute to the increased nutrients we observe in the excreta in our model(43).

Failure to thrive, where pwCF fail to gain weight and grow at the expected rate, is a more systemic pathology with a strong intestinal component(7, 42, 44). *Cftr* knockdown flies have significantly reduced energy stores, with lower levels of whole-body TAG and glucose at both 2 and 4 weeks of age (Fig 1E-H, S1C-F). The reduction of TAG levels is robust at both 2 and 4 weeks of age while the reduction of glucose stores is more apparent at 4 weeks of age. This reduction in whole body energy stores is not due to a developmental defect as inducing *Cftr* knockdown in adult flies using the temperature sensitive Gal80^{ts} repressor also leads to reduced whole body TAGs and glucose (S1 G-H). Furthermore, the reduction in whole body energy stores is not due to reduced food intake as the CF gut model flies consume similar amounts of food to WT flies over 24 hrs and in 30 minutes after starvation (S1I-J). This decrease in whole body energy stores is consistent with a failure to thrive phenotype. As the CF gut model only has reduced *Cftr* expression in the midgut, it may be useful in studying gut-specific contributions to the failure to thrive outcome.

Finally, pwCF have reduced lifespans, although they have improved dramatically in recent years due to the availability of better treatments(45). Our model fly shows that loss of *Cftr*

in the gut alone is sufficient to reduce the lifespan of the fly, highlighting the importance of CFTR function in the gut (Fig 1I, S1K). Overall, these results show that loss of *Cftr* in the enterocytes recapitulates many hallmarks of CF in the gastrointestinal system.

Single nuclei analysis of CF model guts

To further characterize the CF gut model, we performed snRNA-seq on the midgut of WT and CF model gut flies. The sn-RNA-seq analysis recovered 3,669 nuclei for WT and 4,166 for CF midguts that were clustered into 21 clusters annotated using the marker genes from the previously published cell atlas of the *Drosophila* gut(46, 47) (Fig 2A). These clusters include multiple enterocyte (EC) clusters that map along the *Drosophila* digestive tract and show transcriptional similarity to mammalian enterocytes(48) (S2A). The posterior EC (pEC) clusters show high transcriptional similarity to the mature distal enterocytes while the anterior ECs (aEC) cluster only shows moderate similarity to mature proximal enterocytes (S2A). The middle ECs (mECs), copper cells, and large flat cells (LFC) which reside in the middle of the *Drosophila* midgut show moderate similarity to mammalian EC clusters (S2A). The *Drosophila* midgut does not contain specific goblet or paneth cells but the aEC clusters are transcriptionally similar to paneth cells and multiple EC clusters express genes specific to goblet cells in the mammalian gut (S2A). The *Drosophila* enteroendocrine cells show strong sequence similarity to the mammalian enteroendocrine cells. Finally, the *Drosophila*, intestinal stem cells (ISCs), enteroblasts (EBs), and adult differentiating enterocytes are similar to the mammalian stem cells, transit amplifying cells, and enterocyte progenitor cells (S2A).

UMAP analysis of the sn-RNA-seq data does not identify any unique clusters in the CF model guts, however there are a number of clusters that are over or under-represented in the CF

model (Fig 2A-B, S2B). This includes increased ISCs, which is consistent with the hyperplasia previously described in the *Drosophila* CF model gut(26). Furthermore, there are a significant number of differentially expressed genes (DEGs) between WT and CFTR deficient guts across all identified cell clusters (Fig 2C, File S1). Together these results indicate substantial differences in the transcriptional profile and cellular composition between WT and CF model guts.

Interestingly, many secreted peptides are differentially expressed indicating that the CF gut model may be a good model to study the crosstalk between the CF gut and other organs (Fig 2D, S2C, File S2). Among the upregulated secreted proteins in the CF model midguts are several that have also been identified as key factors secreted by Yki-activated gut tumors involved in tumorigenesis and communication with other organs (*Impl2*, *Pvf1*, *Itp*, and *Upd3*)(49, 50) (S2D). This overlap suggests that the CF model gut may exhibit a predisposition toward intestinal tumorigenesis similar to pwCF who are at increased risk of gastrointestinal cancers(11, 13, 39, 40).

In addition to the expected increase of cells in the ISCs cell clusters(26) there is a redistribution of cells in anterior and posterior EC cell clusters (Fig 2A-B, S2B). In the CF preferred anterior EC cluster, one of the top 5 differentially expressed secreted peptides is Acetylcholine esterase (Ace, human AChE) (Fig 2D). *Ace* expression is increased overall in CF model guts but is particularly apparent in the anterior EC clusters (Fig 3A, S3A-B). We confirmed increased *Ace* expression in our CF model guts by RT-qPCR analysis of whole guts (S3C).

Ace hydrolyzes acetylcholine into acetate and choline thereby inhibiting cholinergic signaling. Cholinergic signaling has recently been shown to be required for recovery of the

intestinal epithelium after damage and for maintaining intestinal barrier function in *Drosophila*(27, 28). Furthermore, cholinergic signaling has been shown to increase CFTR activity but there are no studies showing CFTR function affecting cholinergic signaling(31-34). Therefore, we investigated the importance of increased *Ace* expression in our CF gut model.

Reduced Cholinergic signaling in the CF Gut Model

As Ace degrades acetylcholine (ACh), the agonist of cholinergic receptors, increased *Ace* expression should decrease sensitivity to ACh and limit cholinergic signaling(27). Cholinergic signaling has been proposed to use Ca^{2+} as a secondary messenger to modulate the mammalian intestinal epithelium(51). Therefore, to test for cholinergic sensitivity in the *Cftr* deficient midguts we visualized Ca^{2+} by conditionally expressing the Ca^{2+} indicator GCaMP7c(52) in ECs and performed *ex vivo* live imaging(27). We found that Ca^{2+} levels in CF model guts were reduced in response to ACh, indicating that CF model guts had a dampened response to ACh stimulation compared to WT guts (Fig 3B-C).

Cholinergic receptors include both muscarinic and nicotinic receptors, however previous sequencing of the *Drosophila* gut only identifies the presence of certain nicotinic receptor subunits and no muscarinic subunits (53, 54). Therefore, we treated the *Drosophila* midguts with nicotine, which activates nicotinic receptors without being degraded by Ace(55). Nicotine treatment increases Ca^{2+} levels in WT and to a lesser extent in CF model guts (S3D-E). This suggests that cholinergic signaling may be impaired at the receptor level in the CF model gut in addition to the increased *Ace* expression. In our snRNA-seq data set nicotinic receptors have low coverage and were therefore filtered out of the differential expression analysis (File S3). However, when the nicotinic receptors are included in the analysis, we observe a trend towards

reduction in overall nicotinic receptor subunit gene expression (S3F-G). We confirmed this overall reduction in nicotinic receptor subunits by RT-qPCR (S3H). We observe a significant decrease in beta1, beta2, alpha5 and alpha7 nicotinic receptor subunits with no change in the alpha4 and alpha5 subunits and were not able to detect the alpha6 subunit mRNA via RT-qPCR (S3H). These data confirm that cholinergic signaling is reduced in the CF model by both reduced levels of nicotinic receptor subunits and by increased *Ace* expression.

To test the importance of *Ace* expression in the CF gut models sensitivity to cholinergic signaling we used the *Mex*-Gal4 (enterocyte specific driver) together with the Gal4 repressor Tubulin-Gal80^{TS} to drive expression of both *Ace*^{RNAi} and *Cftr*^{RNAi} in adult *Drosophila* for 2 weeks (S4). When *Ace* levels are reduced in the CF background the response to ACh is increased to WT levels (Fig 3D-E). This result indicates that reducing *Ace* expression in CF model guts is sufficient for rescuing sensitivity to cholinergic signaling even if nicotinic receptor subunit levels are also lower in the CF model. This is likely because *Ace* knockdown in the CF background reduce *Ace* levels below WT levels (S3I). Therefore, if decreased cholinergic signaling is important for CF pathophysiology reducing *Ace* expression should alter CF phenotypes in the *Drosophila* model.

Increasing cholinergic signaling in CF model gut rescues several CF phenotypes

Recent work has demonstrated that loss of cholinergic signaling after damage leads to increased proliferation of ISCs and a failure to return to homeostasis(27). Therefore, we examined whether *Ace* expression affected the hyperplasia present in the CF model gut. Indeed, *Ace* knockdown in the CF model gut reduced proliferation in the gut indicating that decreased

cholinergic signaling contributes to the increased proliferation observed in the CF intestine (Fig 4A).

We also found that increasing cholinergic signaling by reducing *Ace* levels in the CF model gut rescued the excretion rate indicating that cholinergic signaling can regulate intestinal transit in the CF model (Fig 4B). Reducing *Ace* expression in the CF model gut was also sufficient for rescuing both the whole-body TAG stores and the malabsorption of nutrients observed in the CF model gut at 2 weeks of age (Fig 4C-F).

Recently cholinergic signaling has been linked to intestinal barrier function in the *Drosophila* gut(28). As there is evidence of increased intestinal permeability in pwCF(56), we tested whether the CF model gut had decreased intestinal barrier function. To test intestinal barrier function, we performed a Smurf assay, where flies are fed a blue food dye that in healthy guts is impermeable to the intestinal barrier. When intestinal barrier function is impaired the blue dye leaks into the hemolymph and the fly turns blue (Smurf)(57). We found that CF model guts have decreased barrier function demonstrated by the increase percentage of Smurf flies at 35 days of age (Fig 4G). Importantly, intestinal barrier integrity is rescued by increasing cholinergic signally via *Ace* knockdown in the gut (Fig 4G).

Altogether these results indicate that the reduction in cholinergic signaling observed in CF model guts contributes to multiple CF pathologies.

Fkh regulates *Ace* transcription in CF model gut

As *Ace* RNA levels are changed in the CF model gut, we performed a screen of transcription factors to identify how *Ace* expression is regulated downstream of loss of CFTR function. To be included in the screen the transcription factor had to 1) have expression in the

single cell data where *Ace* is expressed (S5A) and 2) have potential binding sites as assessed by the TF2G database (Table S1)(58). We identified 18 putative transcription factors (TFs) and used RNAi to test their ability to regulate *Ace* transcription in the *Cftr* deficient background (*MyoTS*> $Cftr^{RNAi}$, TF^{RNAi}) by quantifying *Ace* levels (S5B). The top 2 hits with the lowest *Ace* expression in the CF background were *fork head* (*fkh*) RNAi lines (Fig 5A). In *Drosophila* Fkh has been shown to regulate ISC proliferation and expression of nutrient transporters in the intestine(59, 60). Interestingly, the mammalian ortholog FOXA1/A2 regulates expression of CFTR and other transmembrane proteins important for regulating ion homeostasis in the intestinal epithelium(35, 36). Additionally, *fkh* expression has the highest correlation with *Ace* expression in the aEC2 CF cell cluster of the transcription factors we tested (S5C). Furthermore, Fkh has 2 ChIP-Seq peaks identified at the *Ace* promoter in an embryonic ChIP-seq data set in a region identified as a cis-regulatory module (CRM)(61) for *Ace* (S5D-E). In addition to the Fkh peaks at the *Ace* promoter there are an additional 2 Fkh ChIP-seq peaks in the intronic regions of *Ace.* These intronic binding sites could also be important for regulation of *Ace* transcription especially since Fkh mammalian ortholog, FOXA1, has been shown to regulate *CFTR* expression through intronic binding sites (62-64). Together these data support but do not confirm direct regulation of *Ace* transcription by Fkh as Fkh is 1) expressed in cells that express *Ace* (S5A,C) 2) has the ability to bind to the *Ace* promoter and intronic regions (S5D-E) and 3) knockdown of *Fkh* reduces *Ace* mRNA levels (Fig 5A, S5F). Therefore, we investigated Fkh activity and function in the CF model guts.

As there is minimal difference in the expression of *fkh* between WT and CF midguts in our single cell data and that Fkh activity is known to be regulated by nuclear translocation(60, 65), we examined Fkh nuclear localization. We used confocal microscopy to image the

localization of Fkh in the anterior midguts, the region with highest *Ace* expression in the *Cftr* deficient guts. We found increased nuclear localization of the Fkh protein in the nuclei of CF model compared to WT guts consistent with increased Fkh transcriptional activity (Fig 5B-C, S5G-H). Fkh nuclear localization can be inhibited by phosphorylation by mTOR(60, 65). Consistent with increased Fkh nuclear localization there is decreased mTOR activity, measured by phospho-4EBP levels in anterior midguts, in the CF model gut compared to WT guts (Fig S5I-J).

If Fkh is regulating *Ace* transcription, we expect Fkh manipulation to also modulate CF pathologies. Indeed, reducing *fkh* expression lowered ISC proliferation, increased intestinal motility, increased whole body TAG stores, and increased intestinal barrier integrity in the CF model guts (Fig 5D-F,J). Interestingly, *fkh* knockdown in the *Cftr* deficient background does not fully rescue the nutrient malabsorption phenotype as shown by no change in the amount of glucose or protein remaining in the excreta and only partial reduction of the TAG levels in the excreta (Fig 5G-H). This is the one phenotype tested that does not phenocopy *Ace* knockdown, likely due to other transcriptional targets of Fkh, such as nutrient transporters, also being downregulated (60). These results suggest that increased Fkh nuclear localization downstream of CFTR loss of function regulates CF pathophysiology likely through increasing *Ace* expression.

Discussion

We show that the *Drosophila* CF intestinal model recapitulates several clinical pathologies of CF, including poor intestinal motility, nutrient malabsorption, reduced whole body energy stores, and decreased intestinal barrier function. Additionally, we performed snRNA-seq on *Cftr* deficient and WT midguts uncovering an upregulation of *acetylcholine*

esterase (*Ace*) expression in *Cftr* deficient enterocytes. This upregulation in *Ace* results in a decreased sensitivity to acetylcholine in *Cftr* deficient enterocytes. Importantly, we demonstrate that increasing cholinergic sensitivity in *Cftr* deficient enterocytes by *Ace* knockdown rescues several clinical pathologies of CF. Finally, we identify the FOXA1/A2 ortholog Fkh as a putative transcription factor for *Ace*, that has increased nuclear localization in the *Cftr* deficient midguts (Fig 6).

Previous work has shown that cholinergic signaling can increase CFTR activity(31, 32) , but it has not been shown previously that CFTR can affect cholinergic signaling. Here, we demonstrate that loss of CFTR function leads to an increase in *Ace* expression and a reduction in the guts sensitivity to cholinergic signaling, indicating that there may be reciprocal regulation between cholinergic signaling and CFTR activity. This is interesting as it has been recently demonstrated in *Drosophila* that cholinergic signaling is required for a return to homeostasis after damage to the gut(27). This decrease in cholinergic signaling potential may be preventing the gut from returning to homeostasis from the damage being done by loss of CFTR. This may be because the CF gut is constantly being damaged and it may be energetically unfavorable to be constantly returning to normal homeostasis, but further studies are required to explore this hypothesis.

Additionally, we demonstrate that increasing the sensitivity to cholinergic signaling in CF model guts rescues many pathological phenotypes. Although decreasing *Ace* expression can increase cholinergic signaling in ECs it is possible that some or all of the rescue of CF pathologies with *Ace* knockdown is not cell autonomous. Ace reduces the levels of acetylcholine in the intercellular space and can affect cholinergic signaling in any nearby cell type that expresses nicotinic receptors, such as the EEs and visceral muscle. Further work will be required

to definitively show which cell types are most affected by the increase in *Ace* expression in the CF model ECs. However, whether decreasing *Ace* expression in the CF model ECs is working cell autonomously or increasing cholinergic signaling in other cell types, it still improves many CF related phenotypes. Cholinergic signaling is already being investigated as a therapeutic target for diseases of intestinal inflammation such as IBD(29, 30, 66) which shares many GI symptoms with CF(67, 68). This work suggests AChE inhibition may also be therapeutically beneficial for patients with CF as well.

We also show that *Ace* transcription downstream of *Cftr* loss of function is at least in part regulated by an increase in Fkh activity. We provide evidence including Fkh ChIP-seq peaks at the *Ace* promoter and intronic region and a transcriptional response of *Ace* to Fkh depletion, that supports direct regulation of *Ace* by Fkh. However, further work such as mutational analysis would be needed to confirm direct regulation of Ace by Fkh and to fully characterize how Fkh regulates Ace transcription.

Interestingly, the human orthologs of Fkh FOXA1/FOXA2 are known to regulate the expression of CFTR as well as other ion channels important for intestinal cell function(35, 36). Therefore, in the context of ECs with decreased CFTR activity increasing FOXA1/FOXA2 activity could be a compensatory mechanism to try and increase CFTR function. The increase in Fkh activity in the CF model is not due to an increase in *fkh* transcription but instead a result of increased Fkh nuclear localization. We observe evidence of decreased mTOR activity in the CF model gut which is consistent with increased Fkh nuclear localization(60, 65). However, further studies are required to determine if the decrease in mTOR activity is cell autonomous and directly related to the loss of CFTR function. However, while Fkh activity is required for increased *Ace* transcription in the *Drosophila* CF model, it is likely not sufficient to increase *Ace*

mRNA levels. Treatment of flies with rapamycin, which has been demonstrated to increase Fkh nuclear localization(60, 65), does not increase *Ace* mRNA levels after 10 or 20 days of treatment, although it is increased after 50 days, indicating that Fkh activity alone is not sufficient to increase *Ace* transcription in the midgut(69). Therefore, other transcription factors may also be important for the increased transcription of *Ace* observed in the CF model. Additional studies are needed to investigate whether any of the other transcription factors that reduced *Ace* levels in our screen are important in the context of CF. Finally, it will be important to test if this interaction between CFTR loss of function, increased Fkh activity and increased *Ace* expression is conserved in mammalian systems, as FOXA1/A2 and AChE could be therapeutically relevant targets.

We performed snRNA-Seq to compare the intestines of WT and the CF *Drosophila* model. While no unique cell clusters were identified in the CF model, we observed an increase in ISCs and newly differentiated ECs, along with a shift in EC cluster composition. The expansion of the stem cell population aligns with the increased risk of cancer in pwCF(11, 13, 39, 40). We further investigated the upregulation of *Ace* in the CF gut, prompted by recent studies highlighting the role of cholinergic signaling in maintaining intestinal epithelial homeostasis in *Drosophila*(*28*). In addition, we identified a substantial number of differentially expressed genes (DEGs) across all cell types, presenting numerous opportunities for future investigation. Notably, many differentially expressed secreted peptides may play a role in inter-organ communication. Together with observed changes in whole-body metabolite levels and lifespan, these findings suggest that the *Drosophila* CF model may provide valuable insights into how gut dysfunction influences systemic physiology.

Our study further establishes *Drosophila* as a useful model to study CF. Importantly, CF clinical outcomes are only partially determined by CFTR mutations and are influenced by other genetic modifiers(70-73). Many of these modifiers have been identified by GWAS studies while others are hypothesized based on interaction with CFTR or other experimental evidence(70-73). However, in most cases, these putative modifiers have not been validated and studied in detail(70-73). This work highlights the potential of *Drosophila* for investigating potential CF genetic modifiers. For example, the fly model can be used to screen which of these potential genetic modifiers alter CF pathophysiology. Understanding how CF modifiers affect physiology could lead to new drug targets that could be beneficial to all CF patients regardless of the type of CFTR mutations. Similarly, *Drosophila* would be an ideal model for a first pass to screen chemical libraries for potential CF therapeutics as a relatively cheap *in vivo* model with clinically relevant phenotypes.

Methods

Fly lines

The following fly stocks were used in this study: Drivers from Perrimon lab stocks: mex1-Gal4(74) (mex), mex1-Gal4 Tubulin-Gal80TS (*mex*TS), Myo31DF^{NP0001}-Gal4 (myo1A-Gal4)(75), Myo1A-Gal4 Tubulin-Gal80TS(*myo1A*TS).

UAS-RNAi lines from NIG and BDSC Drosophila Stock Centers: UAS-Cftr^{RNAi}- NIG Stocks: 5789R-1 & 5789R-4, UAS-Ace^{RNAi}- BDSC 25958, UAS-Luciferase^{RNAi}-BDSC 31603 UAS-fkh^{RNAi}- BDSC 27072, UAS-fkh^{RNAi} #2- BDSC 58059, UAS-Blimp-1^{RNAi}- BDSC57479, UAS-Ken^{RNAi}- BDSC-34739, UAS-CF2^{RNAi}- BDSC 57256, UAS-Jim^{RNAi}- BDSC 42662, UAS-br^{RNAi}-BDSC 33641, UAS-Eip93F^{RNAi} BDSC 57868, UAS-Xrp1^{RNAi}- BDSC 51054, UAS-nub^{RNAi}-

BDSC 28338, UAS-GATAd^{RNAi}- BDSC 34640, UAS-Cic^{RNAi}- BDSC 25995, UAS-Ets21c^{RNAi}- BDSC 39069, UAS-br^{RNAi} #2- BDSC 27172, UAS- rel^{RNAi}- BDSC 28943, UAS-pdm2^{RNAi}- BDSC 29453, UAS-pdm2^{RNAi} #2- BDSC 50665, UAS-rel^{RNAi} #2- BDSC 35661, UAS-CG5953^{RNAi}- BDSC 57543, UAS-CG5953RNAi #2- BDSC 57287, UAS-GATAd^{RNAi}-BDSC 33747, UAS-BTb-viiRNAi- BDSC 28912, UAS-Trl^{RNAi}- BDSC 40940, UAS-TrlRNAi #2- BDSC 41582, UAS-Eip74ef- BDSC 29353.

Excretion assay

Flies were fed overnight on lab food with 2 g/100 ml FD&C Blue Dye (12-15 flies per vial for female and 15-20 flies per vial for male). After overnight feed they were moved to 5 ml culture tube without food for 2 hrs (female) or 1 hr 45 minutes (males), time points where the flies have not completely cleared the food from their midguts. Excreta was collected in 400 ul of .05% PBST and 100 ul was used in triplicate to measure blue absorbance at 625 nm using the SpectraMax Paradigm Multi-mode microplate reader (Molecular Devices). A standard curve was made with serial dilutions of the FD&C Blue Dye in .05% PBS and values were normalized to WT for each experiment.

Whole body metabolite measurements

For each replicate 5 flies (females) or 8 flies (males) were collected in eppendorph tubes containing 1.0 mm Zirconium Oxide Beads (Next Advance Lab Products—ZROB10) and frozen on dry ice and stored at -80C. Samples were moved to ice and 500 μL of ice-cold PBS with 0.05% Triton-X-100(Sigma) was added to the tubes. Homogenization was carried out using a TissueLyser II (QIAGEN) for 2-3 cycles of 30 seconds each, at an oscillation frequency of 30

Hz/s. Tubes were centrifuged for 1 minute at 3500 g to remove debris, and the homogenate was immediately used for glucose, protein, and TAG quantification. Quantifications were performed using a SpectraMax Paradigm Multi-mode microplate reader (Molecular Devices). For protein measurements, 5 μL of the homogenate was mixed with 200 μL of the BCA Protein Assay Kit in triplicate (Pierce BCA Protein Assay Kit), followed by incubation for 30 minutes at 37°C with gentle shaking in 96-well Microplates (Greiner Bio-One) and measuring absorbance at 562nm. Glucose quantification involved mixing 10 μL of homogenate with 100 μL of Infinity Glucose Hexokinase Reagent in triplicate (Thermo Fisher Scientific—TR15421), incubating for 30 minutes at 37°C in 96-well Microplates UV-Star (Greiner Bio-One – 655801) with gentle shaking and measuring 340nm. For triglycerides, 5 μL of the homogenate was mixed with 150 μL of Triglycerides Reagent in triplicate (Thermo Fisher Scientific—TR22421) and incubated for 10 minutes at 37°C in 96-well Microplates (Greiner Bio-One) with gentle shaking and absorbance was measured at 520 nm. Values were calculated from standard curves using seven serial dilutions (1:1) of BSA (Pierce BCA Protein Assay Kit), glycerol standard solution (Sigma), or glucose standard solution (Sigma). Glucose and TAG levels were normalized to BCA protein levels and then normalized to WT levels for each independent cross.

Glucose in excreta

Flies were fed overnight on lab food supplemented with 1 g/ L FD&C Blue dye with 15-20 flies per vial. Flies were transferred to 5 ml culture tubes with 200 ul of lab food supplemented with 1 g/ L FD&C Blue Dye for 6 hr. Excreta was collected in 200 ul of .05% PBST and transferred to a 96 well microplate (Greiner Bio-One – 655801) and absorbance was measured at 625 nm using the SpectraMax Paradigm Multi-mode microplate reader (Molecular Devices). A standard curve

was made with serial dilutions of the FD&C Blue Dye in .05% PBS. Glucose quantification was performed as in whole body metabolite measurements and glucose levels were normalized to total excreta amount (625 nm) absorbance before being normalized to the WT condition in each experiment.

TAG and Protein in Excreta

Flies were fed overnight on lab food supplemented with 1 g/ L FD&C Blue dye with 60 flies per bottle. Flies were transferred to 5 ml culture tubes with 200 ul of lab food supplemented with 1 g/ L FD&C Blue Dye for 4 hr. Excreta was collected in 200 ul of .05% PBST and transferred to a 96 well microplate (Greiner Bio-One – 655801) and absorbance was measured at 625 nm using the SpectraMax Paradigm Multi-mode microplate reader (Molecular Devices). A standard curve was made with serial dilutions of the FD&C Blue Dye in .05% PBS. TAG quantification was performed as in whole body metabolite measurements section. Protein levels were measured via BCA assay as described in whole body metabolite measurements section. TAG and protein levels were normalized to total excreta amount (625 nm) absorbance before being normalized to the WT condition in each experiment.

Feeding Assay

24hr. Feeding Assay: The amount of food consumed over a 24hr period was measured using the DIETS assay (76). 25 flies were place in a vial with agar plug (as water source) and a small amount of food (100ul) was placed in an eppendorph tube cap. The cap with food was affixed with tape to the side of the fly vial. The flies were acclimatized to the system for 24hrs before being transferred to a new vial with agar plug with a weighed eppendorph tube cap with 100 ul

of food. After 24 hrs of consumption the food was weighed again. Empty vials with food caps were used as evaporation controls. Food intake per fly was calculated as (change in weight-evaporation controls change in weight)/ number of flies.

30 minute blue dye feeding assay: Flies were starved overnight before being put on standard lab food containing 1g/100ml FD and C blue dye for 30 minutes. 5 flies with heads removed were homogenized in 600ul of .05% PBST and tubes were were centrifuged for 1 minute at 3500 g to remove debris. 100 ul was used in triplicate per replicate to measure blue absorbance at 625 nm using the SpectraMax Paradigm Multi-mode microplate reader (Molecular Devices). A standard curve was made with serial dilutions of the FD&C Blue Dye in .05% PBS and values were normalized to WT for each experiment.

Lifespan assay

15 (females) or 20 (males) 2-4 day old adult flies were placed in vials on standard laboratory food. Flies were flipped every other day and vials were scored for percent survival.

Smurf assay

Smurf assay was performed as previously described(57). Briefly 10-15 female flies were raised on standard fly food and flipped every 2 days for 33 days before being put on standard fly food supplemented with 2.5 g per 100 ml of FD & C blue dye for 2 days. At 35 days each vial was scored for percentage smurf flies under a dissection microscope.

RNA isolation, RT and quantitative PCR

For RNA isolation, 10-15 adult guts were dissected, and tissues were homogenized in TRIzol reagent (Ambion). The supernatant was collected and processed using Direct-zol RNA MicroPrep columns (Zymo Research) following the manufacturer's protocol. Reverse transcription was performed using the iScript cDNA Synthesis Kit (Bio-Rad). Quantitative real-time PCR (qRT-PCR) was carried out on a CFX96 Real-Time System (Bio-Rad) using iQ SYBR Green Supermix (Bio-Rad). qRT-PCR reaction volume used was 10 µl (2 µl 5 µM Primer pair mix+ 5 µ 2x SYBR Green+ 3 µl cDNA). Relative mRNA levels were determined using the ΔΔCt method, with mRNA levels normalized to Rpl32.

qPCR primers:

Gene	Forward	Reverse
Ace	AGGTGCATGTCTACACGGG	ACGTTGGTGTTGGGGTTCC
nAchRa3	ATGAAGTGGTTTCAAGTGACCAT	CAAATCGTCGTACAATCGTTTCG
nAchRa4	TGGGTGTGGACCTATCTGAAT	AAGTATGGTTCGTCGCAACAA
nAChRa5	CAGCAACTCACAACACTGCAA	CCGTGGTTGGCTACATCCTC
nAchRa7	ATGCTGGTCTATGGCCTGG	GAGTAGCCGCTTCTCATGGG
nAchRb1	TGGAGTCTTCCTGCAAATCCT	GCCACAAGCACCAGGATG
nAchRb3	ATGACGACGACTCCCAAGATA	AAGAAGCATCCCCATTAGCATTT
Rpl32	AGCATACAGGCCCAAGATCG	TGTTGTCGATACCCTTGGGC

Single-nuclei RNA-seq

***Single-nucleus suspension and FACS*:** Single-nucleus suspension was conducted as previously described(47). Briefly, 70 guts per condition were dissected in cold Schneider's medium, flash-frozen and stored at -80°C. Prior to FACs sorting, samples were spun down and Schneider's medium was exchanged with homogenization buffer [250mM Sucrose, 10mM Tris pH8, 25mM KCl, 5mM MgCl, 0.1% Triton-X, 0.5% RNasin Plus (Promega, N2615), 50x protease inhibitor (Promega G6521), 0.1mM DTT]. Using 1ml dounce (Wheaton 357538), nuclei were released by 20 loose pestle strokes and 40 tight pestle strokes while keeping samples on ice and avoiding

foam. Next, nuclei were filtered through 5 ml cell strainer (40 μm), and using 40 μm Flowmi (BelArt, H13680-0040). Nuclei were centrifuged, resuspended in PBS/0.5%BSA with 0.5% RNase inhibitor, filtered again with 40 μm Flowmi and stained with DRAQ7 Dye (Invitrogen, D15106). Single nuclei were sorted with Sony SH800Z Cell Sorter at PCMM Flow Cytometry Facility at Harvard Medical School and 100k nuclei per sample were collected in PBS/BSA buffer.

10x genomics and sequencing: Single nuclei RNA-seq libraries were prepared using the Chromium Next GEM Single Cell 3' Library and Gel Bead Kit v3.1 according to the 10xGenomics protocol. Approximately 16,500 nuclei were loaded on Chip G with an initial concentration of 700 cells/µl based on the 'Cell Suspension Volume Calculator Table'. Sequencing was conducted with Illumina NovaSeq 6000 at Harvard Medical School Biopolymers Facility.

10x data processing: Raw sequencing data were aligned to the *Drosophila melanogaster* reference genome (BDGP6.32, Ensembl release 104) using 10x Genomics Cell Ranger v7.1.0. Low quality nuclei with less than 500 Unique Molecular Identifiers (UMI) were filtered out. The default clustering and uniform manifold approximation and projection (UMAP) generated by 10X Loupe Browser was used to cluster cells. Cell types were manually annotated using the top marker genes from each cluster. The filtered count matrix and metadata were loaded into R (v4.4.0) and further processing was performed using the default Seurat workflow (v5.2.1). Differential gene expression analysis was performed using a Mann Whitney-U test with a cut-off of p-value < 0.05 and abs(Log2FC) > .5 and percent expression > 1%.

Normalized expression violin plots and heatmaps were generated using Seurat, ggplot2 (v3.5.2), ComplexHeatmap (2.24.0) and pheatmap (v1.0.12). hdWGCNA (v0.4.05) was used to create metacells for which Pearson correlation tests were performed for candidate transcription factors and Ace expression.

Cell type comparison between *Drosophila* and mammalian intestinal epithelium.

We used DIOPT (release 7, score>3) (77) to map mouse genes to *Drosophila* orthologs. The *Drosophila* orthologs of markers identified in various cell types from mammalian datasets were grouped respectively as cell type specific gene sets. Next, we compared the cell type specific gene sets from the mammalian study (48) and the cell type markers from *Drosophila (46)*. P-value of enrichment was calculated based on the hypergeometric distribution and the similarity of Drosophila markers with mammalian markers is reflected by the negative log10 of the P values.

GCaMP7c live imaging

GCaMP7c live imaging was performed as previously described(27). Guts were dissected in fresh HL3 buffer (1.5mM Ca2+, 20mM MgCl2, 5mM KCl, 70mM NaCl,10mM NaHCO3, 5mM HEPES, 115mM Sucrose, 5mM Trehalose) and placed in eight-well clear bottom cell culture chamber slides with HL3. Guts were stabilized with a Nylon mesh (Warner instruments, 64-0198) and paper clips cut in small identical pieces. ACh and Nicotine sensitivity assay: ACh and Nicotine sensitivity assay was done using LSM780 and LSM980 microscopes with 40x water objective lens. Each frame (~2.5 sec/frame) is the maximum projection of 5-6 z-stacks

(2.96µm/z) and was acquired with 488nm excitation for GFP. 5mM Acetylcholine (Acetylcholine Chloride, Sigma A2661) or 1.33 mM Nicotine (Sigma, N3876) were added at the 10th frame (~25 sec) For Figure 3B-C an old aliquot of Acetylcholine was used at 10mM after testing response in WT midguts to a range of concentrations, when new aliquot was purchased 5mM concentration was used after testing a range of concentrations in WT guts as giving a similar response to previous experiment. All images were taken from similar areas in the Anterior midgut between R1-R2. Fiji was used for assembly and calculation of fluorescence per frame. DF/F0 = Ffr-F0/ F0. Ffr is the fluorescence per frame and F0 (baseline fluorescence) is the average fluorescence intensity of the first 9 frames (fr1-fr9).

PH3+ counts

Guts were dissected and fixed in 4% PFA for 20 minutes. They were washed 3x in .1% PBST and incubated for 1 hr at RT in 5% Normal Goat Serum in .1%PBST. Guts were incubated for overnight with rabbit anti-pH3 (Millipore #06-570; 1:3000). Guts were then washed for 30 minutes 3x in .1% PBST then incubated for 2hrs at RT with secondary antibody, Alexa Fluor 555-conjugated goat anti-rabbit IgG (1:200) and DAPI (1:3000). The guts were then washed 3X in .1%PBST for 30 minutes and mounted in VECTASHIELD antifade mounting media (Vector Laboratories). Slide genotype was blinded and PH3+ nuclei were counted with an epifluorescence microscope.

Fkh nuclear localization

Guts were dissected and fixed in 4% PFA for 20 minutes. They were washed 3x in .1% PBST and incubated for 1 hr at RT in 5% Normal Goat Serum in .1%PBST. Guts were incubated for 2

days at 4C with Rab-anti-FKH (60, 78-80) (1:100)(gift from Dr. Chandrasekaran, St. Mary's College of California) in 5% Normal Goat Serum in .1%PBST. Guts were then washed for 30 minutes 3x in .1% PBST then incubated overnight in secondary antibody, Alexa Fluor 555-or 647 conjugated goat anti-rabbit IgG (1:200) and DAPI (1:3000). The guts were then washed 3X in .1%PBST for 30 minutes and mounted in antifade mounting media. Fluorescence was imaged using W1 Yokogawa spinning disk, Nikon inverted Ti2 confocal microscope. Percent nuclear localization was calculated on maximum intensity projections in Fiji.

Phospho-4EBP1 Staining

Guts were dissected and fixed in 4% PFA for 30 minutes. They were washed 3x in .1% PBST and incubated for 1 hr at RT in 5% Normal Goat Serum in .1%PBST. Guts were incubated for 2 days at 4C with Rab-anti-p4EBP1 (1:800) (CST 2855S) in 5% Normal Goat Serum in .1%PBST. Guts were then washed for 30 minutes 3x in .1% PBST then incubated overnight in secondary antibody, Alexa Fluor 555-or 647 conjugated goat anti-rabbit IgG (1:200) and DAPI (1:3000). The guts were then washed 3X in .1%PBST for 30 minutes and mounted in antifade mounting media. Fluorescence was imaged using W1 Yokogawa spinning disk, Nikon inverted Ti2 confocal microscope. Average staining intensity was calculated on maximum intensity projections in Fiji.

Statistics and Reproducibility

Prism (https://www.graphpad.com/scientific-software/prism/) or ggplot2 was used to create graphs as well as to perform statistical analysis. Statistical tests are indicated in figure legends. No statistical analysis was conducted to determine sample sizes. Randomization was not

performed. Blinding experiments were conducted during mitotic division counts. No data were excluded. Confocal images shown in figures are representative of two to 4 independent experiments with similar result.

Data Sharing/ Resource Availability

The scRNA-seq portal for data mining is available at https://www.flyrnai.org/scRNA/. Raw RNA-seq reads and processed data files have been deposited in the NCBI Gene Expression Omnibus (GEO) database under accession code: GSE300597.

Author Contributions.

Conceptualization: Elizabeth A. Lane, Norbert Perrimon
Data Curation: Yanhui Hu, Weihang Chen, Mujeeb Qadiri
Formal Analysis: Elizabeth A. Lane, Afroditi Petsakou, Mujeeb Qadiri
Funding Acquisition: Elizabeth A. Lane, Norbert Perrimon
Investigation: Elizabeth A. Lane, Afroditi Petsakou, Ying Liu
Methodology: Elizabeth A. Lane, Afroditi Petsakou, Ying Liu
Project Administration: Elizabeth A. Lane, Norbert Perrimon
Software: Weihang Chen, Mujeeb Qadiri, and Yanhui Hu
Supervision: Norbert Perrimon
Visualization: Elizabeth A. Lane, Ying Liu, Mujeeb Qadiri, and Yanhui Hu
Writing – Original Draft Preparation: Elizabeth A. Lane
Writing – Review & Editing: Norbert Perrimon, Afroditi Petsakou, Ying Liu

This article is subject to HHMI's Open Access to Publications policy. HHMI lab heads have previously granted a nonexclusive CC BY 4.0 license to the public and a sublicensable license to HHMI in their research articles. Pursuant to those licenses, the author-accepted manuscript of this article can be made freely available under a CC BY 4.0 license immediately upon publication.

Acknowledgments: Confocal imaging was conducted at MicRoN Facility at Harvard Medical School, and we thank Paula Montero Llopis for advice. We also thank Biopolymers Facility and Computing facilities and PCMM Flow Cytometry Facility at Harvard Medical School. We thank Sudhir Gopal Tattikota for his expertise on 10x snRNA-seq. We thank Muhammad Ahmad for advice on image analysis. We thank DRSC/TRiP, NiG and the Bloomington Stock Center for fly lines. We thank Dr. Chandrasekaran for providing the anti-Fkh antibody.

Financial Disclosure Statement

This work was funded by NIH F32 Ruth-Kirschstein Postdoctoral Fellowship (NIDDK) 5F32DK130290-03 (https://www.niddk.nih.gov/), CF Foundation Postdoctoral Research Fellowship Award LANE21F0-00816F221(https://www.cff.org/) which provided salary for E.A.L.. N.P. is an investigator of the Howard Hughes Medical Institute (https://www.hhmi.org/).

The funders had no role in study design, data collection and analysis, decision to publish, or preparation of the manuscript.

Declaration of Interest

The authors have declared that no competing interests exist.

Declaration of generative AI and AI-assisted technologies in the writing process

During the preparation of this work the author(s) used ChatGTP in order to polish certain sections of text. After using this tool/service, the author(s) reviewed and edited the content as needed and take(s) full responsibility for the content of the publication.

References

1. Cutting GR. Cystic fibrosis genetics: from molecular understanding to clinical application. Nat Rev Genet. 2015;16(1):45-56.
2. Gregory RJ, Cheng SH, Rich DP, Marshall J, Paul S, Hehir K, et al. Expression and characterization of the cystic fibrosis transmembrane conductance regulator. Nature. 1990;347(6291):382-6.
3. Farkas B, Tordai H, Padanyi R, Tordai A, Gera J, Paragi G, et al. Discovering the chloride pathway in the CFTR channel. Cellular and molecular life sciences : CMLS. 2019.
4. Riordan JR, Rommens JM, Kerem B, Alon N, Rozmahel R, Grzelczak Z, et al. Identification of the cystic fibrosis gene: cloning and characterization of complementary DNA. Science (New York, NY). 1989;245(4922):1066-73.
5. Grubb BR, Gabriel SE. Intestinal physiology and pathology in gene-targeted mouse models of cystic fibrosis. The American journal of physiology. 1997;273(2 Pt 1):G258-66.
6. Mall M, Grubb BR, Harkema JR, O'Neal WK, Boucher RC. Increased airway epithelial Na+ absorption produces cystic fibrosis-like lung disease in mice. Nature medicine. 2004;10(5):487-93.
7. Brownell JN, Bashaw H, Stallings VA. Growth and Nutrition in Cystic Fibrosis. Semin Respir Crit Care Med. 2019;40(6):775-91.
8. Elborn JS. Cystic fibrosis. The Lancet. 2016;388(10059):2519-31.
9. Ooi CY, Durie PR. Cystic fibrosis from the gastroenterologist's perspective. Nat Rev Gastroenterol Hepatol. 2016;13(3):175-85.
10. Brown SD, White R, Tobin P. Keep them breathing: Cystic fibrosis pathophysiology, diagnosis, and treatment. JAAPA : official journal of the American Academy of Physician Assistants. 2017;30(5):23-7.
11. Maisonneuve P, Marshall BC, Knapp EA, Lowenfels AB. Cancer risk in cystic fibrosis: a 20-year nationwide study from the United States. Journal of the National Cancer Institute. 2013;105(2):122-9.
12. Billings JL, Dunitz JM, McAllister S, Herzog T, Bobr A, Khoruts A. Early colon screening of adult patients with cystic fibrosis reveals high incidence of adenomatous colon polyps. Journal of clinical gastroenterology. 2014;48(9):e85-8.
13. Niccum DE, Billings JL, Dunitz JM, Khoruts A. Colonoscopic screening shows increased early incidence and progression of adenomas in cystic fibrosis. Journal of cystic fibrosis : official journal of the European Cystic Fibrosis Society. 2016;15(4):548-53.
14. Moshiree B, Freeman AJ, Vu PT, Khan U, Ufret-Vincenty C, Heltshe SL, et al. Multicenter prospective study showing a high gastrointestinal symptom burden in cystic fibrosis. J Cyst Fibros. 2023;22(2):266-74.
15. Moshiree B, Freeman AJ, Vu PT, Khan U, Ufret-Vincenty C, Heltshe SL, et al. Multicenter prospective study showing a high gastrointestinal symptom burden in cystic fibrosis. Journal of Cystic Fibrosis. 2023;22(2):266-74.

695 16. Marsh R, Dos Santos C, Hanson L, Ng C, Major G, Smyth AR, et al. Tezacaftor/Ivacaftor
696 therapy has negligible effects on the cystic fibrosis gut microbiome. Microbiol Spectr.
697 2023;11(5):e0117523.
698 17. Marsh R, Santos CD, Yule A, Dellschaft NS, Hoad CL, Ng C, et al. Impact of extended
699 Elexacaftor/Tezacaftor/Ivacaftor therapy on the gut microbiome in cystic fibrosis. J Cyst Fibros.
700 2024;23(5):967-76.
701 18. Calthorpe RJ, Goodchild N, Gleetus V, Premakumar V, Hayee B, Elliott Z, et al. A
702 grumbling concern: A survey of gastrointestinal symptoms in cystic fibrosis in the modulator
703 era. NIHR Open Res. 2023;3:18.
704 19. Schwarzenberg SJ, Vu PT, Skalland M, Hoffman LR, Pope C, Gelfond D, et al.
705 Elexacaftor/tezacaftor/ivacaftor and gastrointestinal outcomes in cystic fibrosis: Report of
706 promise-GI. J Cyst Fibros. 2023;22(2):282-9.
707 20. Wrigley-Carr HE, van Dorst JM, Ooi CY. Intestinal dysbiosis and inflammation in cystic
708 fibrosis impacts gut and multi-organ axes. Medicine in Microecology. 2022;13:100057.
709 21. Bertolini A, Nguyen M, Zehra SA, Taleb SA, Bauer-Pisani T, Palm N, et al. Prominent role
710 of gut dysbiosis in the pathogenesis of cystic fibrosis-related liver disease in mice. Journal of
711 Hepatology. 2024;81(3):429-40.
712 22. Price CE, O'Toole GA. The Gut-Lung Axis in Cystic Fibrosis. J Bacteriol.
713 2021;203(20):e0031121.
714 23. Miguel-Aliaga I, Jasper H, Lemaitre B. Anatomy and Physiology of the Digestive Tract of
715 Drosophila melanogaster. Genetics. 2018;210(2):357-96.
716 24. Capo F, Wilson A, Di Cara F. The Intestine of Drosophila melanogaster: An Emerging
717 Versatile Model System to Study Intestinal Epithelial Homeostasis and Host-Microbial
718 Interactions in Humans. Microorganisms. 2019;7(9).
719 25. Medina A, Bellec K, Polcowñuk S, Cordero JB. Investigating local and systemic intestinal
720 signalling in health and disease with Drosophila. Disease models & mechanisms. 2022;15(3).
721 26. Kim K, Lane EA, Saftien A, Wang H, Xu Y, Wirtz-Peitz F, et al. Drosophila as a model for
722 studying cystic fibrosis pathophysiology of the gastrointestinal system. Proc Natl Acad Sci U S A.
723 2020;117(19):10357-67.
724 27. Petsakou A, Liu Y, Liu Y, Comjean A, Hu Y, Perrimon N. Cholinergic neurons trigger
725 epithelial Ca(2+) currents to heal the gut. Nature. 2023;623(7985):122-31.
726 28. Katheder NS, Browder KC, Chang D, De Maziere A, Kujala P, van Dijk S, et al. Nicotinic
727 acetylcholine receptor signaling maintains epithelial barrier integrity. Elife. 2023;12.
728 29. Serafini MA, Paz AH, Nunes NS. Cholinergic immunomodulation in inflammatory bowel
729 diseases. Brain Behav Immun Health. 2022;19:100401.
730 30. Uwada J, Nakazawa H, Muramatsu I, Masuoka T, Yazawa T. Role of Muscarinic
731 Acetylcholine Receptors in Intestinal Epithelial Homeostasis: Insights for the Treatment of
732 Inflammatory Bowel Disease. International Journal of Molecular Sciences. 2023;24(7):6508.
733 31. Maouche K, Medjber K, Zahm J-M, Delavoie F, Terryn C, Coraux C, et al. Contribution of
734 α7 nicotinic receptor to airway epithelium dysfunction under nicotine exposure. Proceedings of
735 the National Academy of Sciences. 2013;110(10):4099-104.
736 32. Billet A, Hanrahan JW. The secret life of CFTR as a calcium-activated chloride channel. J
737 Physiol. 2013;591(21):5273-8.

738 33. Mall M, Bleich M, Schürlein M, Kühr J, Seydewitz HH, Brandis M, et al. Cholinergic ion
739 secretion in human colon requires coactivation by cAMP. The American journal of physiology.
740 1998;275(6):G1274-81.
741 34. Jakab RL, Collaco AM, Ameen NA. Characterization of CFTR High Expresser cells in the
742 intestine. Am J Physiol Gastrointest Liver Physiol. 2013;305(6):G453-65.
743 35. Gosalia N, Yang R, Kerschner JL, Harris A. FOXA2 regulates a network of genes involved
744 in critical functions of human intestinal epithelial cells. Physiol Genomics. 2015;47(7):290-7.
745 36. Kerschner JL, Gosalia N, Leir SH, Harris A. Chromatin remodeling mediated by the
746 FOXA1/A2 transcription factors activates CFTR expression in intestinal epithelial cells.
747 Epigenetics. 2014;9(4):557-65.
748 37. Parisi GF, Papale M, Pecora G, Rotolo N, Manti S, Russo G, et al. Cystic Fibrosis and
749 Cancer: Unraveling the Complex Role of CFTR Gene in Cancer Susceptibility. Cancers (Basel).
750 2023;15(17).
751 38. Anton-Păduraru DT, Murgu AM, Bozomitu LI, Mîndru DE, Iliescu Halițchi CO, Trofin F, et
752 al. Diagnosis and Management of Gastrointestinal Manifestations in Children with Cystic
753 Fibrosis. Diagnostics (Basel). 2024;14(2).
754 39. Garg M, Ooi CY. The Enigmatic Gut in Cystic Fibrosis: Linking Inflammation, Dysbiosis,
755 and the Increased Risk of Malignancy. Curr Gastroenterol Rep. 2017;19(2):6.
756 40. de Souza Furtado J, de Almeida Brasiel PG, Luquetti S. Profile of the intestinal microbiota
757 of patients with cystic fibrosis: A systematic review. Clin Nutr ESPEN. 2023;55:400-6.
758 41. Henen S, Denton C, Teckman J, Borowitz D, Patel D. Review of Gastrointestinal Motility
759 in Cystic Fibrosis. Journal of Cystic Fibrosis. 2021;20(4):578-85.
760 42. Li L, Somerset S. Digestive system dysfunction in cystic fibrosis: challenges for nutrition
761 therapy. Dig Liver Dis. 2014;46(10):865-74.
762 43. Li X, Rommelaere S, Kondo S, Lemaitre B. Renal Purge of Hemolymphatic Lipids Prevents
763 the Accumulation of ROS-Induced Inflammatory Oxidized Lipids and Protects Drosophila from
764 Tissue Damage. Immunity. 2020;52(2):374-87.e6.
765 44. Giglio L, Candusso M, D'Orazio C, Mastella G, Faraguna D. Failure to thrive: the earliest
766 feature of cystic fibrosis in infants diagnosed by neonatal screening. Acta Paediatrica.
767 1997;86(11):1162-5.
768 45. McBennett KA, Davis PB, Konstan MW. Increasing life expectancy in cystic fibrosis:
769 Advances and challenges. Pediatr Pulmonol. 2022;57 Suppl 1(Suppl 1):S5-s12.
770 46. Hung RJ, Hu Y, Kirchner R, Liu Y, Xu C, Comjean A, et al. A cell atlas of the adult
771 Drosophila midgut. Proc Natl Acad Sci U S A. 2020;117(3):1514-23.
772 47. Li H, Janssens J, De Waegeneer M, Kolluru SS, Davie K, Gardeux V, et al. Fly Cell Atlas: A
773 single-nucleus transcriptomic atlas of the adult fruit fly. Science (New York, NY).
774 2022;375(6584):eabk2432.
775 48. Haber AL, Biton M, Rogel N, Herbst RH, Shekhar K, Smillie C, et al. A single-cell survey of
776 the small intestinal epithelium. Nature. 2017;551(7680):333-9.
777 49. Liu Y, Saavedra P, Perrimon N. Cancer cachexia: lessons from Drosophila. Disease
778 models & mechanisms. 2022;15(3).
779 50. Xu W, Li G, Chen Y, Ye X, Song W. A novel antidiuretic hormone governs tumour-induced
780 renal dysfunction. Nature. 2023;624(7991):425-32.

781 51. Hirota CL, McKay DM. Cholinergic regulation of epithelial ion transport in the
782 mammalian intestine. Br J Pharmacol. 2006;149(5):463-79.
783 52. Dana H, Sun Y, Mohar B, Hulse BK, Kerlin AM, Hasseman JP, et al. High-performance
784 calcium sensors for imaging activity in neuronal populations and microcompartments. Nat
785 Methods. 2019;16(7):649-57.
786 53. Dutta D, Dobson AJ, Houtz PL, Gläßer C, Revah J, Korzelius J, et al. Regional Cell-Specific
787 Transcriptome Mapping Reveals Regulatory Complexity in the Adult Drosophila Midgut. Cell
788 Rep. 2015;12(2):346-58.
789 54. Marianes A, Spradling AC. Physiological and stem cell compartmentalization within the
790 Drosophila midgut. Elife. 2013;2:e00886.
791 55. Jiang J, Li X, Hu AF, Zhou GJ, Gao YH, Xu C, et al. Nicotine and neuronal nicotinic
792 acetylcholine receptors: unraveling the mechanisms of nicotine addiction. Front Neurosci.
793 2025;19:1670883.
794 56. Hallberg K, Grzegorczyk A, Larson G, Strandvik B. Intestinal permeability in cystic fibrosis
795 in relation to genotype. J Pediatr Gastroenterol Nutr. 1997;25(3):290-5.
796 57. Martins RR, McCracken AW, Simons MJP, Henriques CM, Rera M. How to Catch a Smurf?
797 - Ageing and Beyond… In vivo Assessment of Intestinal Permeability in Multiple Model
798 Organisms. Bio Protoc. 2018;8(3).
799 58. Hu Y, Rodiger J, Liu Y, Gao C, Liu Y, Qadiri M, et al. TF2TG: an online resource mining the
800 potential gene targets of transcription factors in Drosophila. Genetics. 2025.
801 59. Lan Q, Cao M, Kollipara RK, Rosa JB, Kittler R, Jiang H. FoxA transcription factor Fork
802 head maintains the intestinal stem/progenitor cell identities in Drosophila. Dev Biol.
803 2018;433(2):324-43.
804 60. Bolukbasi E, Khericha M, Regan JC, Ivanov DK, Adcott J, Dyson MC, et al. Intestinal Fork
805 Head Regulates Nutrient Absorption and Promotes Longevity. Cell Rep. 2017;21(3):641-53.
806 61. Rivera J, Keränen SVE, Gallo SM, Halfon MS. REDfly: the transcriptional regulatory
807 element database for Drosophila. Nucleic Acids Res. 2019;47(D1):D828-d34.
808 62. Yin S, NandyMazumdar M, Paranjapye A, Harris A. Cross-talk between enhancers,
809 structural elements and activating transcription factors maintains the 3D architecture and
810 expression of the CFTR gene. Genomics. 2022;114(3):110350.
811 63. Yang R, Kerschner JL, Gosalia N, Neems D, Gorsic LK, Safi A, et al. Differential
812 contribution of cis-regulatory elements to higher order chromatin structure and expression of
813 the CFTR locus. Nucleic Acids Res. 2016;44(7):3082-94.
814 64. Kerschner JL, Harris A. Transcriptional networks driving enhancer function in the CFTR
815 gene. Biochem J. 2012;446(2):203-12.
816 65. Varma D, Bülow MH, Pesch Y-Y, Loch G, Hoch M. Forkhead, a new cross regulator of
817 metabolism and innate immunity downstream of TOR in Drosophila. Journal of Insect
818 Physiology. 2014;69:80-8.
819 66. Rahman AA, Stavely R, Pan W, Ott L, Ohishi K, Ohkura T, et al. Optogenetic Activation of
820 Cholinergic Enteric Neurons Reduces Inflammation in Experimental Colitis. Cellular and
821 Molecular Gastroenterology and Hepatology. 2024;17(6):907-21.
822 67. Suzuki H. To establish a treatment for GI symptoms of cystic fibrosis, it is necessary to
823 develop a symptom evaluation tool. United European Gastroenterol J. 2019;7(7):873-4.

824 68. Hayee B, Watson KL, Campbell S, Simpson A, Farrell E, Hutchings P, et al. A high
825 prevalence of chronic gastrointestinal symptoms in adults with cystic fibrosis is detected using
826 tools already validated in other GI disorders. United European Gastroenterol J. 2019;7(7):881-8.
827 69. Lu YX, Regan JC, Eßer J, Drews LF, Weinseis T, Stinn J, et al. A TORC1-histone axis
828 regulates chromatin organisation and non-canonical induction of autophagy to ameliorate
829 ageing. Elife. 2021;10.
830 70. Corvol H, Blackman SM, Boelle PY, Gallins PJ, Pace RG, Stonebraker JR, et al. Genome-
831 wide association meta-analysis identifies five modifier loci of lung disease severity in cystic
832 fibrosis. Nat Commun. 2015;6:8382.
833 71. Paranjapye A, Ruffin M, Harris A, Corvol H. Genetic variation in CFTR and modifier loci
834 may modulate cystic fibrosis disease severity. J Cyst Fibros. 2020;19 Suppl 1(Suppl 1):S10-s4.
835 72. O'Neal WK, Knowles MR. Cystic Fibrosis Disease Modifiers: Complex Genetics Defines
836 the Phenotypic Diversity in a Monogenic Disease. Annu Rev Genomics Hum Genet.
837 2018;19:201-22.
838 73. Shanthikumar S, Neeland MN, Saffery R, Ranganathan S. Gene modifiers of cystic
839 fibrosis lung disease: A systematic review. Pediatr Pulmonol. 2019;54(9):1356-66.
840 74. Phillips MD, Thomas CM. Brush border spectrin is required for early endosome recycling
841 in Drosophila. J Cell Sci. 2006;119(Pt 7):1361-70.
842 75. Brand AH, Perrimon N. Targeted gene expression as a means of altering cell fates and
843 generating dominant phenotypes. Development. 1993;118(2):401-15.
844 76. Thakare MR, Choudhary P, Pydah B, Sunke S, Yadav RSP, Agrawal P, et al. DIETS: a simple
845 and sensitive assay to measure and control the intake of complex solid foods, like high-fat diets,
846 in Drosophila. eLife Sciences Publications, Ltd; 2024.
847 77. Hu Y, Flockhart I, Vinayagam A, Bergwitz C, Berger B, Perrimon N, et al. An integrative
848 approach to ortholog prediction for disease-focused and other functional studies. BMC
849 bioinformatics. 2011;12:357.
850 78. Weigel D, Jürgens G, Küttner F, Seifert E, Jäckle H. The homeotic gene fork head encodes
851 a nuclear protein and is expressed in the terminal regions of the Drosophila embryo. Cell.
852 1989;57(4):645-58.
853 79. Chandrasekaran V, Beckendorf SK. senseless is necessary for the survival of embryonic
854 salivary glands in Drosophila. Development. 2003;130(19):4719-28.
855 80. Abrams EW, Mihoulides WK, Andrew DJ. Fork head and Sage maintain a uniform and
856 patent salivary gland lumen through regulation of two downstream target genes, PH4alphaSG1
857 and PH4alphaSG2. Development. 2006;133(18):3517-27.
858
859

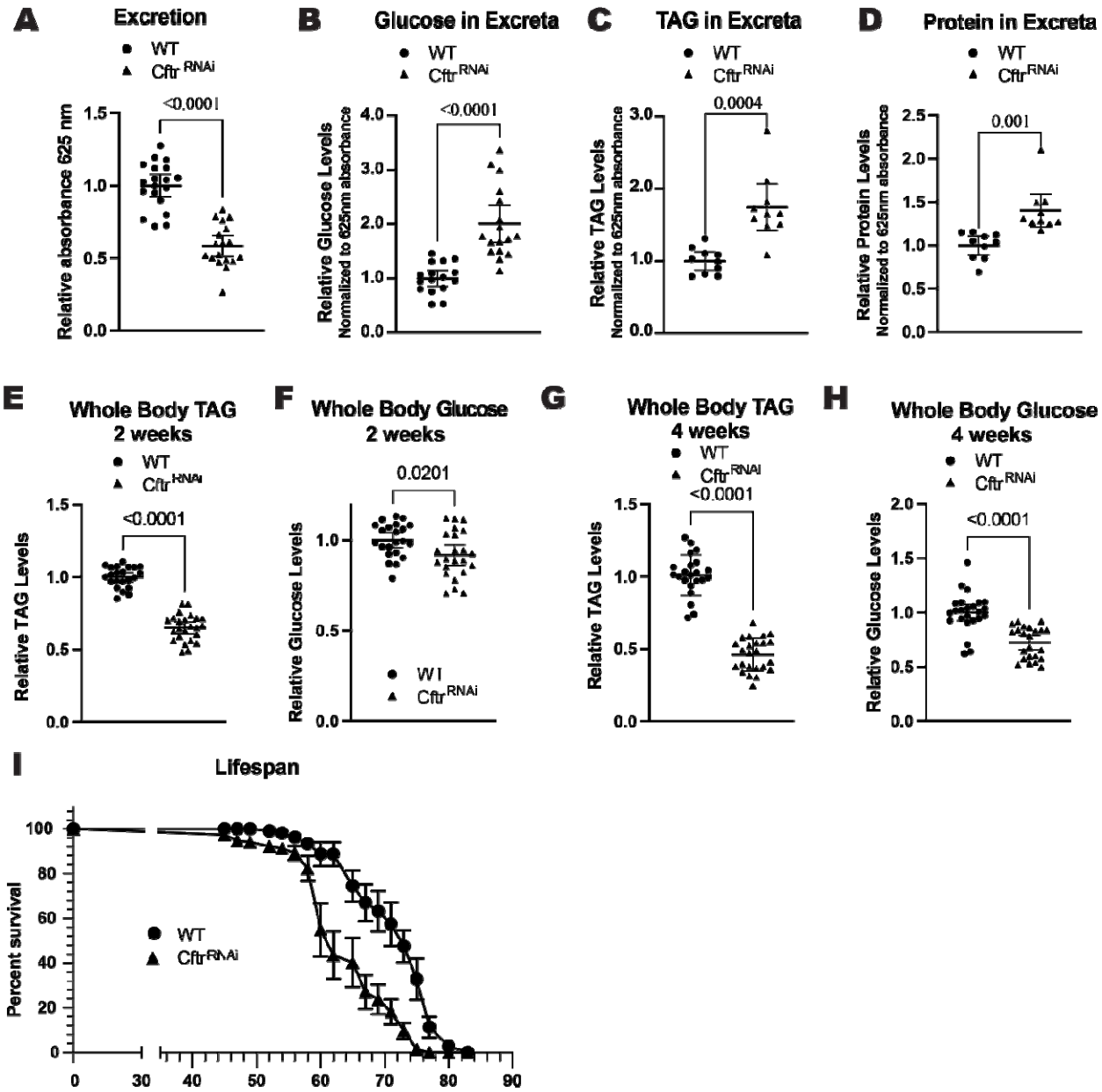

Figure 1. CF model gut recapitulates hallmarks of CF

(**A**) CF model guts have decreased excretion rate compared to WT guts. n= 19 vials of 10-15 females from 3 independent experiments. (**B**) CF model guts have increased glucose in excreta compared to WT flies. n= 16 (WT), 17 (*Cftr*^{RNAi}) vials of 15-20 females from 3 independent experiments. (**C**-**D**) CF model guts have increased TAG (**C**) and protein (**D**) in excreta compared to WT flies. n= 10 vials of 60 females from 3 independent experiments. (**E**) CF model guts have reduced TAG levels at 2 weeks of age compared to WT flies. n= 22 (WT), 24 (*Cftr*^{RNAi}) of 5 pooled females from 4 independent experiments. (**F**) CF model guts have slightly reduced whole body glucose levels at 2 weeks of age compared to WT flies. n= 22 (WT), 24 (*Cftr*^{RNAi}) of 5 pooled females from 4 independent experiments. (**G**) CF model gut flies have reduced whole body TAG levels at 4 weeks of age compared to WT flies. n= 22 (WT), 24 (*Cftr*^{RNAi}) of 5 pooled females from 4 independent crosses. (**H**) CF model gut flies have reduced whole body glucose at

4 weeks of age compared to WT flies. n= 24 (WT), 23 (*Cftr*^{RNAi}) of 5 pooled females from 4 independent crosses. (**A**-**H**) pValues were calculated using the Mann-Whitney test in GraphPad prism. Error bars are mean with 95% CI. (**I**) CF model gut flies have reduced lifespans compared to WT flies. n= 9 (WT), 12 (*Cftr*^{RNAi}) vials with 10-15 females from 2 independent crosses, error bars are mean +/- SEM. (**A**-**I**) WT is *Myo1A* > + and *Cftr*^{RNAi} is *Myo1A* >*UAS-Cftr*^{RNAi}.

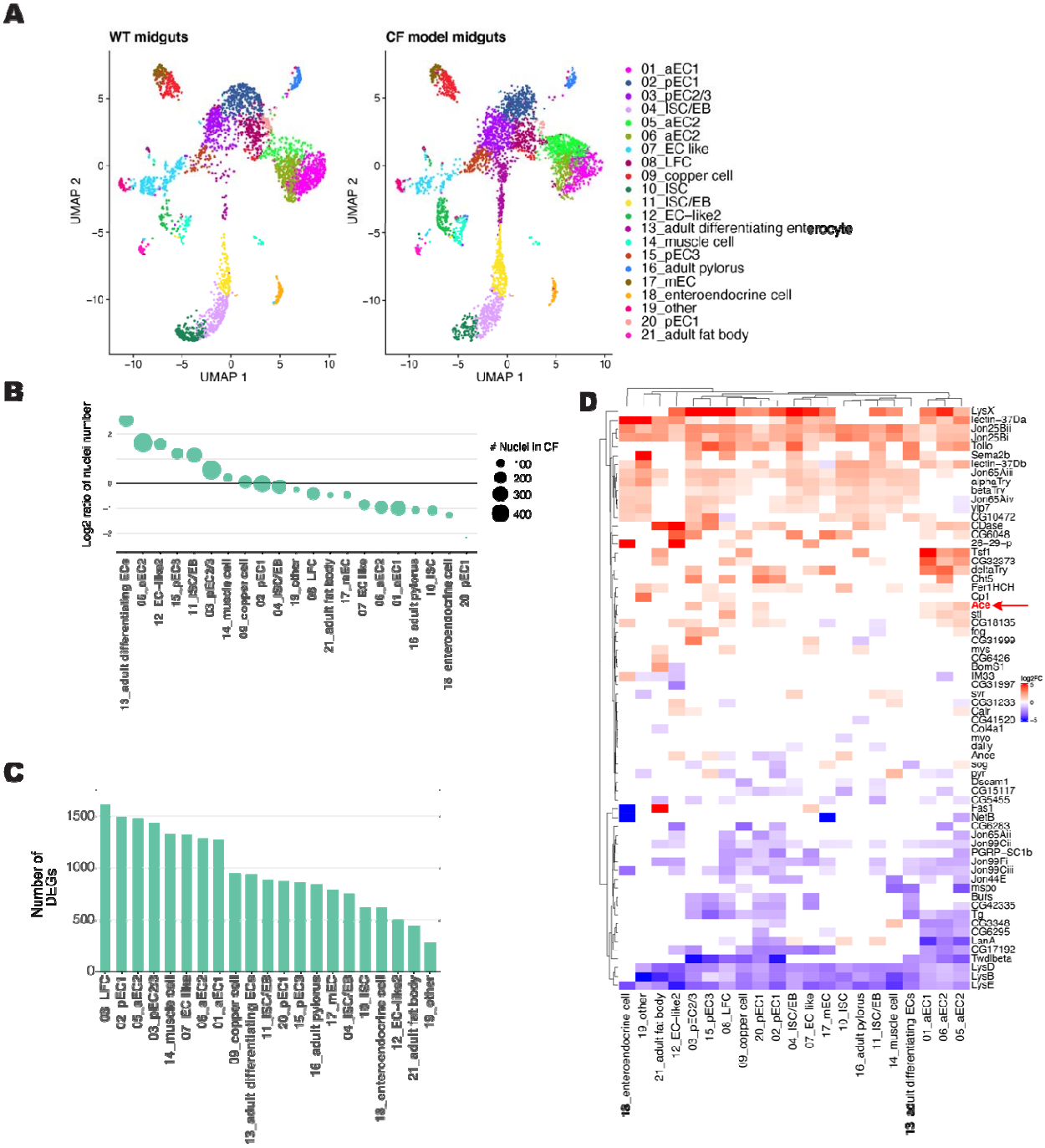

Figure 2. snRNA-Seq of CF model guts

(A) Annotated cell clusters of snRNA-Seq from WT (*Myo1A> +*) and CF (*Myo1A>Cftr*^{RNAi}) midguts, visualized with UMAP. (**B**) Over and underrepresented cell clusters in CF model gut snRNA-seq data set. Size of nuclei represent number of nuclei in CF model gut analysis for indicated cluster. (**C**) Number of differentially expressed genes in each cell cluster between WT and CF model gut snRNA-seq data sets. (**D**) Heat map of the top 5 differentially expressed secreted proteins for each cell type. Color reflects the log2fold change in expression in CF model guts comparing to control per cell cluster.

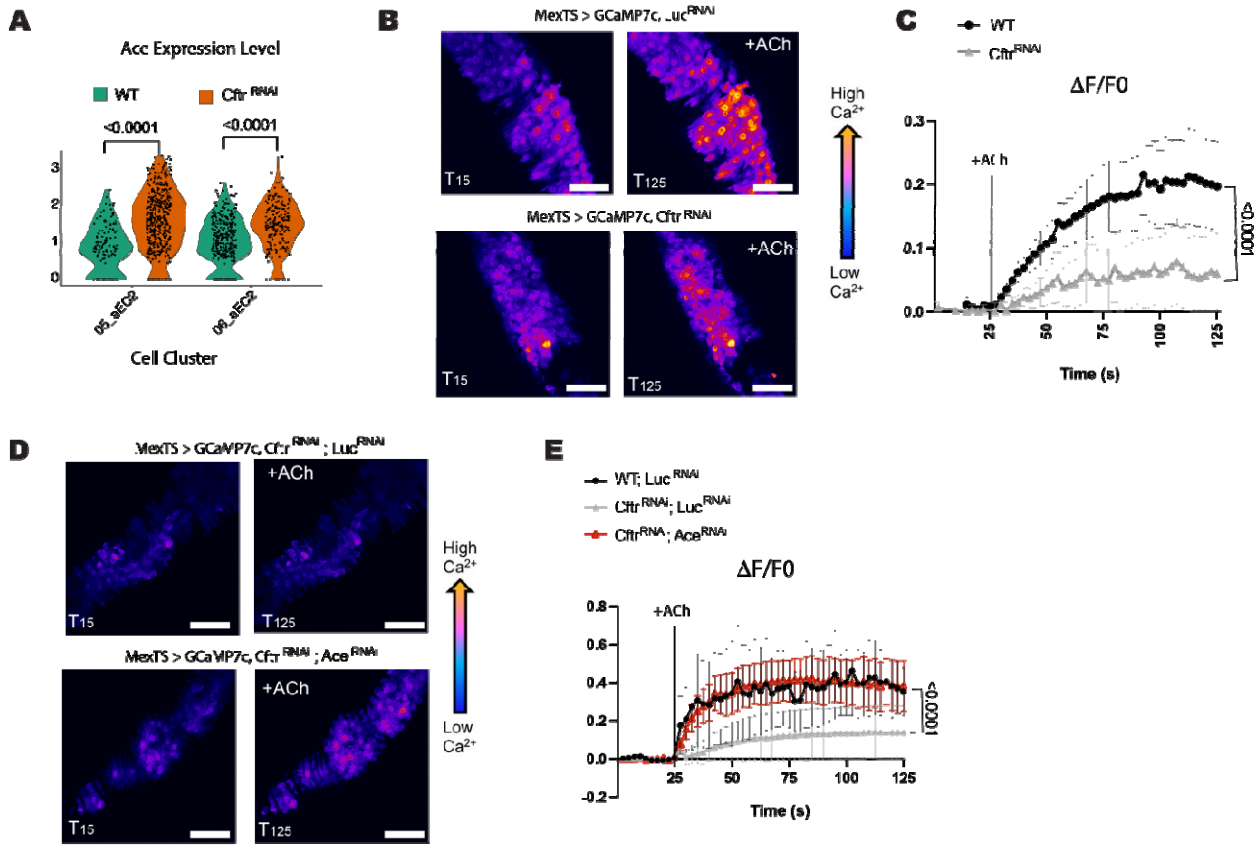

Figure 3. CF model guts have reduced sensitivity to cholinergic signaling

(A) Violin plot of acetylcholine esterase (*Ace*) expression in anterior EC2 cell clusters indicates higher *Ace* expression in CF model guts. Each dot represents expression in a single-nucleus, n=137 (WT) or 479 (*Cftr*^{RNAi}) for 05_aEC2 and n=362 (WT) or 213 (*Cftr*^{RNAi}) for 06_aEC2. pValues were calculated using the Mann-Whitney test in ggplot2. **(B-C)** *Cftr* deficient midguts have reduced sensitivity to acetylcholine (ACh) stimulation as measured by calcium levels in enterocytes. **(B)** Representative images of GCaMP7c fluorescence, in WT (*MexTS > GCaMP7c, LucRNAi*) and *Cftr* deficient guts (*MexTS > GCaMP7c, Cftr*^{RNAi}) before (T15s) or after addition of ACh (T125). Scale bar 50 µm. **(C)** Graph of average relative fluorescent intensity, ΔF/F0, per frame (2.5s per frame) and genotype. n= 9 (WT) and 10 (*Cftr*^{RNAi}) from 4 independent experiments. Error bars are mean +/- SEM. pValue was calculated using the Mann-Whitney test in GraphPad prism. **(D-E)** *Ace* knockdown increases sensitivity to ACh stimulation in *Cftr* deficient enterocytes. **(D)** Representative images of GCaMP7c fluorescence, in *Cftr* deficient (*MexTS > GCaMP7c, Cftr*^{RNAi}*; Luc*^{RNAi}) midguts and *Cftr* deficient guts with *Ace* knockdown (*MexTS > GCaMP7c, Cftr*^{RNAi}*; Ace*^{RNAi}) before (T15s) or after addition of ACh (T125). Scale bar 50 µm. **(E)** Graph of average relative fluorescent intensity, ΔF/F0, per frame (2.5s per frame) and genotype. n= 3 (WT), 5 (*Cftr*^{RNAi}, *Luc*^{RNAi}), 4 (*Cftr*^{RNAi}, *Ace*^{RNAi}) from 3 independent experiment. Error bars are mean +/- SEM. pValues were calculated using 2-way ANOVA with Tukey's multiple comparisons main column effect in GraphPad prism.

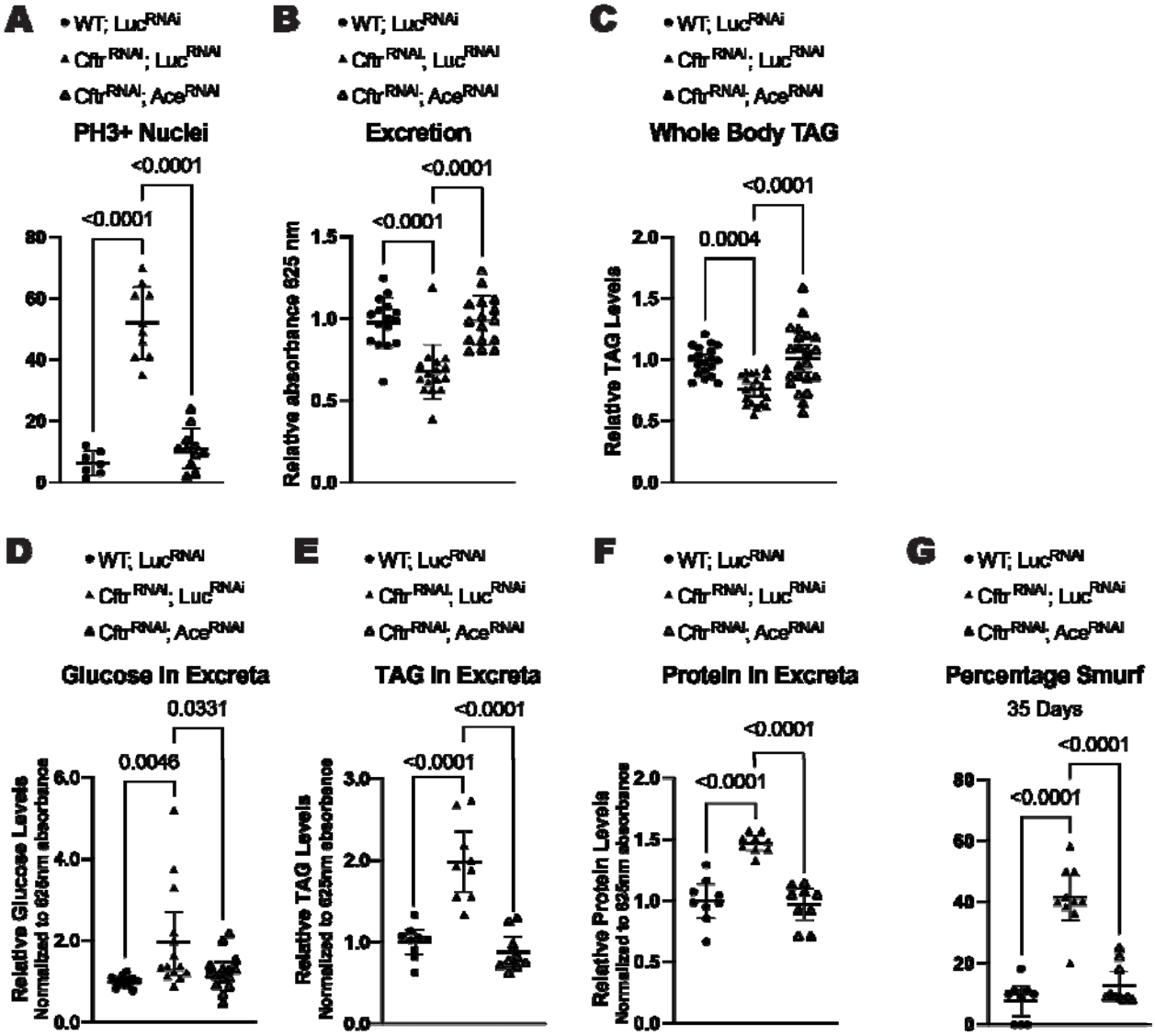

Figure 4. Increasing cholinergic signaling rescues CF phenotypes

(**A**) *Ace* knockdown rescues the increased proliferation seen in CF model guts. n=7 (WT; *Luc*^{RNAi}), 10 (*Cftr*^{RNAi}, *Luc*^{RNAi}), 11 (*Cftr*^{RNAi}*; Ace*^{RNAi}). (**B**) *Ace* knockdown increases intestinal motility as measured by excretion rate in CF model guts. n=16 vials with 9-13 female flies from 3 independent experiments. (**C**) *Ace* knockdown rescues whole body TAG levels at 2 weeks of age in CF model guts. n=19 (WT; *Luc*^{RNAi}), 20 (*Cftr*^{RNAi}, *Luc*^{RNAi}), 22 (*Cftr*^{RNAi}*; Ace*^{RNAi}) of 5 pooled females from 4 independent experiments. (**D**) *Ace* knockdown reduces the amount of glucose remaining in excreta in CF model gut flies. n=14 (WT; *Luc*^{RNAi}), 14 (*Cftr*^{RNAi}, *Luc*^{RNAi}), 15 (*Cftr*^{RNAi}*; Ace*^{RNAi}) vials of 15-20 females from 3 independent experiments. (**E-F**) *Ace* knockdown reduces the amount of TAG (**E**) and protein (**F**) remaining in excreta in CF model gut flies. n=9 vials of 60 flies from 3 independent experiments. (**G**) CF model gut flies have increased intestinal permeability, measured by the presence of normally non-permeable blue dye in the hemolymph at 35 days of age, which is rescued by *Ace* knockdown. n=9 (WT; *Luc*^{RNAi}), 10 (*Cftr*^{RNAi}, *Luc*^{RNAi}), 10 (*Cftr*^{RNAi}*; Ace*^{RNAi}) vials of 9-13 females from 3 independent experiments. (**A-G**) pValues were calculated using ordinary one-way ANOVA with Tukey's multiple

comparisons test in GraphPad prism. Error bars are mean with 95% CI. RNAi constructs were expressed in enterocytes using the enterocyte specific driver *Mex*^{TS} (*Mex-Gal4* with the temperature sensitive gal4 repressor *tubulin gal80*^{TS}) (**S4**).

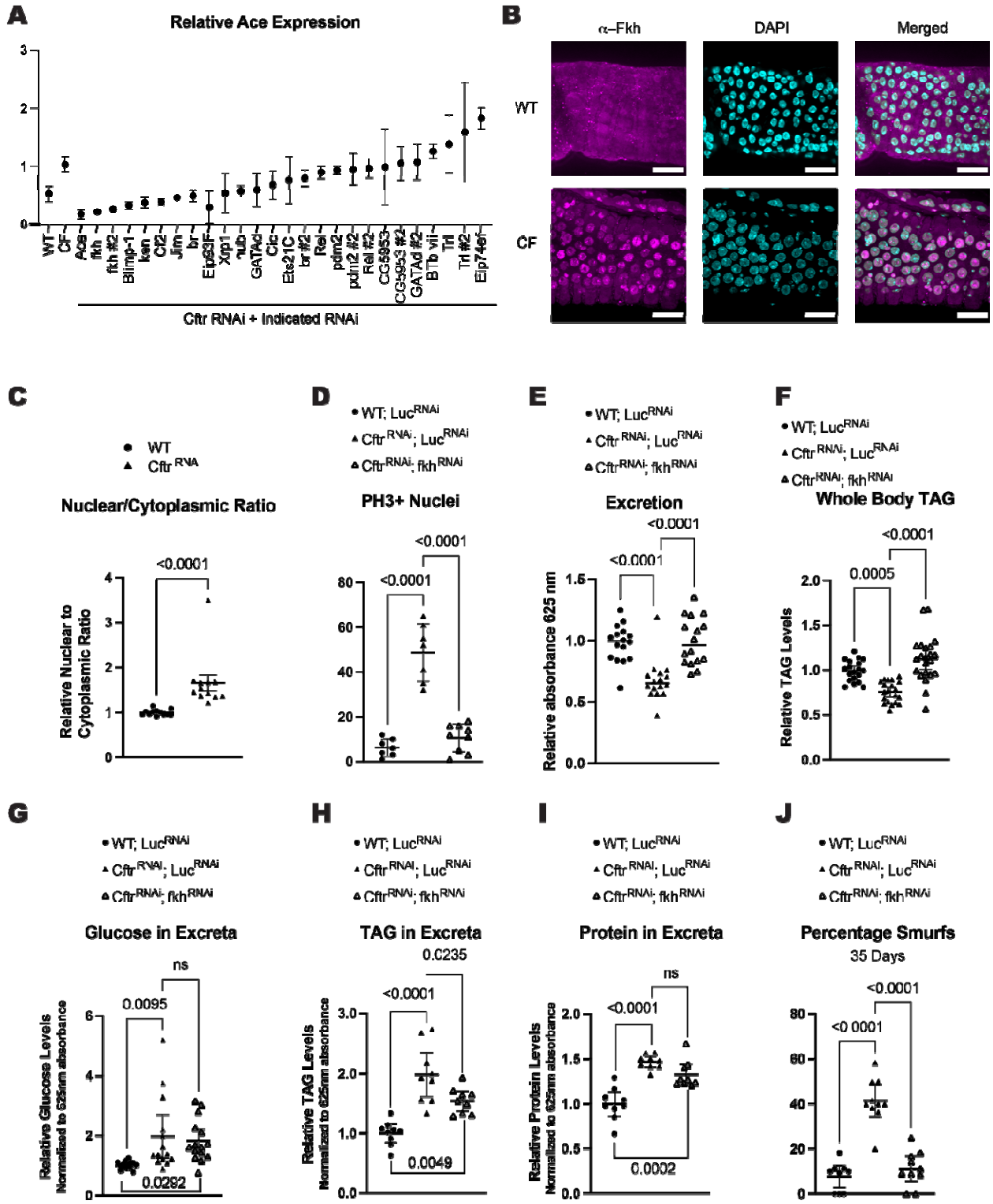

Figure 5. Fkh regulates *Ace* transcription and CF pathologies in the CF model gut

(**A**) Screen of transcription factors identifies Fkh as a candidate transcription factor of *Ace* in the CF model guts. n=2 biological replicates of 15 pooled guts. error bars are mean +/- SD. RNAi constructs were expressed in adult flies for 2 weeks using *Myo*^{TS} (*Myo1A-Gal4, tub-Gal80*^{TS}) driver (S5B). (**B**) Representative images of increased Fkh nuclear localization in CF model guts

compared to WT. scale bars 25µm. (**C**) Fkh has increased nuclear localization in *Cftr* deficient guts. n=12 from 4 independent experiments. pValues were calculated using the Mann-Whitney test in GraphPad prism. Error bars are mean with 95% CI. (**D**) *fkh* knockdown rescues the hyperplasia observed in CF model guts. n= 7 (WT; Luc^{RNAi}), 9 ($Cftr^{RNAi}$, Luc^{RNAi}), 9 ($Cftr^{RNAi}$; fkh^{RNAi}) from 2 independent experiments. (**E**) *fkh* knockdown increases intestinal motility as measured by excretion rate in CF model guts. n=16 vials with 9-13 female flies from 3 independent experiments. (**F**) *fkh* knockdown rescues whole body TAG levels at 2 weeks of age in CF model guts. n=19 (WT; Luc^{RNAi}), 20 ($Cftr^{RNAi}$, Luc^{RNAi}), 22 ($Cftr^{RNAi}$; fkh^{RNAi}) of 5 pooled females from 4 independent experiments. (**G**) *fkh* knockdown does not reduce the amount of glucose remaining in excreta in CF model gut flies. n=14 (WT; Luc^{RNAi}), 14 ($Cftr^{RNAi}$, Luc^{RNAi}), 15 ($Cftr^{RNAi}$; fkh^{RNAi}) vials of 15-20 females from 3 independent experiments. (**H**) *fkh* knockdown reduces TAG levels in the excreta of CF model gut flies. n=9 vials of 60 flies from 3 independent experiments. (**I**) *fkh* knockdown does not reduce the level of protein in the excreta of CF model gut flies. n=9 vials of 60 flies from 3 independent experiments. (**J**) Fkh depletion rescues intestinal barrier function in flies with *Cftr* deficient enterocytes as assessed by percentage smurf flies at 35 days of age. n=9 (WT; Luc^{RNAi}), 10 ($Cftr^{RNAi}$, Luc^{RNAi}), 10 ($Cftr^{RNAi}$; fkh^{RNAi}) vials of 9-13 females from 3 independent experiments. (**D-J**) pValues were calculated using ordinary one-way ANOVA with Tukey's multiple comparisons test in GraphPad prism. Error bars are mean with 95% CI. (**D-J**) Share values for WT; Luc^{RNAi} and $Cftr^{RNAi}$; fkh^{RNAi} with Figure 4 A-E as *Ace* and *fkh* knockdown in CF background were performed at the same time and used the same controls. (**D-J**) RNAi constructs were expressed in enterocytes using the enterocyte specific driver Mex^{TS} (*Mex-Gal4* with the temperature sensitive gal4 repressor *tubulin* $gal80^{TS}$)(S4).

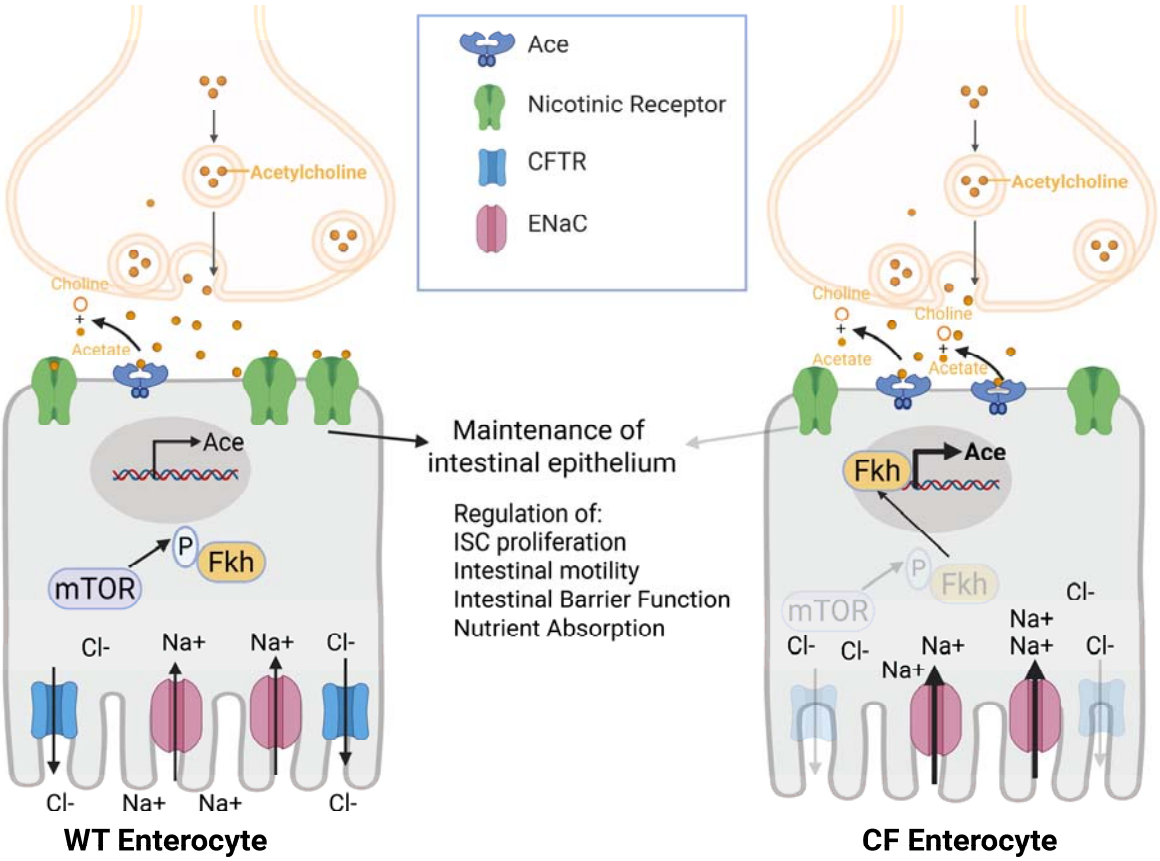

Figure 6. Model Figure

Loss of CFTR function in enterocytes leads to increased Fkh nuclear localization, likely from reduced mTOR activity. Increased Fkh nuclear localization increases *Ace* transcription. Increased Ace degrades acetylcholine, reducing cholinergic signaling in CF enterocytes. This reduction of cholinergic signaling impairs the maintenance of the intestinal epithelium resulting in increased ISC proliferation, decreased intestinal motility, decreased intestinal barrier function and decreased nutrient absorption. This figure was created in BioRender. Lane, L. (2025) https://BioRender.com/r4x91pu.

Supplementary Materials

S1 Appendix: Supplementary Figures S1-S5 and Supplementary Figure Legends
Table S1: Supplementary Table 1- TF2TG
File S1: Differentially Expressed Genes in sn-RNA-seq
File S2: Differentially Expressed Secreted Peptide Genes in sn-RNA-seq
File S3: Average Expression Nicotinic Receptors in sn-RNA-seq
Data S1: Numerical Data Underlying Main Figure Graphs
Data S2: Numerical Data Underlying Supplementary Figure Graphs